Grain Size Distribution under Simultaneous Grain Boundary Migration and Grain Rotation

Selim Esedoḡlu

Department of Mathematics, University of Michigan

December 31, 2015

Abstract

We explore the effects on grain size distribution of incorporating grain rotation into the curvature driven grain boundary migration model of Mullins. A new, extremely streamlined and efficient algorithm allows simulations with large numbers of grains. Some of these simulations yield size distributions and microstructures close to those from recent, atomistic simulations of microstructural evolution using the phase field crystal method that was shown to reproduce experimental size distributions observed in fiber textured, nanocrystalline, thin metallic films.

Keywords: Grain boundary motion, grain size distribution, polycrystalline materials.

1 Introduction

Polycrystalline materials, such as most metals and ceramics, are composed of many single crystal pieces of differing orientation that are known as grains. The shapes and sizes of the grains are well-known to have significant implications for the physical properties of a polycrystalline material, such as its yield strength and conductivity. It is therefore of great practical interest to understand how the sizes and shapes of grains change under common manufacturing processes such as annealing. A well known model for how the grains evolve during annealing was given by Mullins [21]. It is a continuum description of the grain boundaries as a network of surfaces that move via gradient flow to decrease a weighted surface energy. Different versions of this model, often with additional simplifying assumptions, have been studied numerically using a variety of algorithms, such as kinetic Monte Carlo, front tracking, phase field, level sets, and threshold dynamics. Various statistics of grains, such as grain size distribution, grain boundary character distribution, and distribution of the number of neighbors are typically reported in these numerical studies.

In [2, 3], an important discrepancy between the grain size distribution (GSD) obtained from numerical simulations of Mullins' continuum model in 2D and that from experiments with fiber textured nanocrystalline thin films is reported. In this setting, the crystallographic orientation of each grain is described by a single parameter: the angle of rotation about the axis normal to the film. In the reported experiments, grains range in size from 10 to 100 nanometers. The eventual GSD observed differs considerably from that of numerical simulations in having far more very small as well as very large grains compared to the median.

Backofen et. al. [1] carried out simulations of grain growth in two dimensions using the phase field crystal (PFC) model [6]. This is an atomistic model that appears to allow for simulations on time scales beyond what is possible with other atomic scale strategies such as molecular dynamics. As such, it is a promising new tool for very detailed simulations of mesoscale features such as grain boundaries. In [1], the authors report that the resulting GSD resembles the experimentally observed one in [2, 3] far more than the distribution obtained from Mullins' model. They suggest a number of different mechanisms not captured by Mullins' continuum model that may be responsible for the more faithful reproduction of experimental results by the PFC simulations. One of these mechanisms is grain rotation. More recently, incorporating triple junction drag into Mullins' model has been shown in [23] to yield GSDs resembling the experimental results of [2, 3]. Despite being overruled in [3], it thus appears that triple junction drag may be at least partially responsible for the discrepancy in size distribution.

A prominent feature of the results of [1] is that the shapes of the grains in the PFC simulation appear to be quite different from the very regular, almost polygonal grains seen in essentially all two dimensional simulations of Mullins' model (especially with equal surface tensions), computed whether by phase field (e.g. [18]), front tracking (e.g. [15]), or threshold dynamics (e.g. [7]) techniques. In the images and videos of the PFC simulation provided in [1], it is abundantly clear that grain rotation and other fine scale dynamics such as the motion of dislocations frequently lead to elimination of certain grain boundaries resulting in coalescence events that yield many grains with very eccentric, meandering shapes. A natural question is whether elimination of some of the very low energy grain boundaries through such processes may be at least partially responsible in deforming the GSD towards the one reported in [1]. In particular, our goal in this paper is to explore whether grain rotation and coalescences, when incorporated into Mullins' continuum model, may explain the GSDs and unusual microstructures seen in PFC simulations of [1].

To investigate these questions, we propose a new, very simple model of grain rotation that is inspired by [20, 26] and which turns out to be quite similar to a model considered in [12, 19]. Our model can be seen as the natural multiphase version of the one introduced in [26], which uses an additional phase field variable to describe the orientations of grains in the network. This variable, which is observed to be approximately piecewise constant, is part of the gradient descent dynamics and leads to gradual variations

in the orientations of the grains as an additional dissipation mechanism besides the geometric (curvature) flow of the grain boundaries. The numerical treatment of this very interesting model appears to be quite challenging. Here, for our much simpler, multiphase version, we are able to give an extremely streamlined algorithm by leveraging some of the recent advances in numerical treatment of curvature motion in networks [9]. In fact, the basic version of the algorithm can be implemented in literally a few lines of Matlab code; a slightly more sophisticated version allows us to carry out large scale simulations that probe the effects of grain rotation and coalescence on the GSD in Mullins' model.

2 Our Model and Algorithm

Let $\Sigma_j \subset \mathbb{R}^d$ denote the space occupied by the j-th grain in the microstructure. Although the algorithms discussed below work in any dimension and for more general energies, in this study we focus on the two dimensional version of Mullins' model for which the energy of the grain network is given by

$$\sum_{i<j} \sigma(\theta_i, \theta_j) \text{Length}(\Gamma_{i,j}) \tag{1}$$

where $\Gamma_{i,j} = \partial\Sigma_i \cap \partial\Sigma_j$ denotes the boundary between the i-th and j-th grains. The surface tension factor σ is chosen in accordance with the Read-Shockley model [22] along with a Brandon angle [4] that will be denoted θ_* , often taken to be between 15° and 30° :

$$\sigma(\xi, \eta) = \min_{k=1,2,3,\ldots} f\left(\left|\xi - \eta + \frac{k\pi}{4}\right|\right) \tag{2}$$

where

$$f(\theta) = \begin{cases} \frac{\theta}{\theta_*}\left(1 - \log\left(\frac{\theta}{\theta_*}\right)\right) & \text{if } \theta \in [0, \theta_*] \\ 1 & \text{if } \theta > \theta_*. \end{cases} \tag{3}$$

According to Mullins, the dynamics associated with energy (1) is given by L^2 gradient descent for the interfaces, leading to the normal speed

$$v_{i,j} = \mu_{i,j}\sigma(\theta_i, \theta_j)\kappa_{i,j} \tag{4}$$

for interface $\Gamma_{i,j}$. Here $\kappa_{i,j}$ denotes the mean curvature of $\Gamma_{i,j}$, and $\mu_{i,j} > 0$ is a mobility factor. Along triple junctions formed by the meeting of three distinct grains Σ_i , Σ_j , and Σ_k , Herring angle conditions

[13] hold:

$$\sigma(\theta_i, \theta_j) n_{i,j} + \sigma(\theta_j, \theta_k) n_{j,k} + \sigma(\theta_k, \theta_i) n_{k,i} = 0 \tag{5}$$

so that angles formed by normals $n_{i,j}$, $n_{j,k}$, and $n_{k,i}$ to the three interfaces $\Gamma_{i,j}$, $\Gamma_{j,k}$, and $\Gamma_{k,i}$ along the triple junction are determined by their associated surface tensions.

The algorithms used in this study are obtained from a non-local approximation to energy (1): These approximate energies are given by

$$\frac{1}{\sqrt{\delta t}} \sum_{i<j} \sigma(\theta_i, \theta_j) \int_{\Sigma_i} G_{\delta t} * \mathbf{1}_{\Sigma_j} \, dx \tag{6}$$

where G_t denotes the Gaussian kernel in two dimensions

$$G_t(x) = \frac{1}{4\pi t} \exp\left(-\frac{|x|^2}{4t}\right) \tag{7}$$

and $\mathbf{1}_\Sigma(x)$ for a set Σ denotes its characteristic function:

$$\mathbf{1}_\Sigma(x) = \begin{cases} 1 & \text{if } x \in \Sigma, \\ 0 & \text{otherwise.} \end{cases}$$

The width δt of the Gaussian kernel appearing in (6) ends up playing the role of the time step size for our scheme, described below, that approximates gradient descent of (1) in L^2 sense, as prescribed by [21]. Energy (6) has been proposed in [9] and has been shown to converge in a very precise sense (namely, that of Gamma convergence) to energy (1) in the limit $\delta t \to 0^+$. Intuitively, we have

$$\frac{1}{\sqrt{\delta t}} \int_{\Sigma_i} G_{\delta t} * \mathbf{1}_{\Sigma_j} \, dx \approx \text{Length}(\Gamma_{i,j})$$

since the function $\frac{1}{\sqrt{\delta t}} \mathbf{1}_{\Sigma_i} G_{\delta t} * \mathbf{1}_{\Sigma_j}$ approximates a delta function concentrating near $\Gamma_{i,j}$ as $\delta \to 0$. The reason for our interest in this specific – perhaps unusual – approximation of Mullins' energy is that it generates exceptionally simple and efficient algorithms for simulating the gradient descent dynamics associated with (1). Indeed, it has been shown in [9] to lead in a systematic way to the correct multiphase, arbitrary surface tension analogue of a very fast algorithm known as *threshold dynamics* that was originally proposed in [16, 17] for networks with all equal surface tensions (i.e. $\sigma(\theta_i, \theta_j) = 1$ for all i and j). Let us recall the simplest version of the generalization of threshold dynamics to arbitrary surface tensions given in [9]:

Given the initial grain shapes Σ_i^0 and orientations θ_i and a time step size δt, obtain the grain shapes Σ_i^{n+1} at the $(n+1)$-th time step from the grain shapes Σ_i^n at the end of the n-th time step as follows:

1. Compute the convolutions:

$$\phi_i^n = G_{\delta t} * \mathbf{1}_{\Sigma_i^n}. \tag{8}$$

2. Form the comparison functions:

$$\psi_i^n = \sum_{j \neq i} \sigma(\theta_i, \theta_j) \phi_j^n. \tag{9}$$

3. Update the grain shapes:

$$\Sigma_i^{n+1} = \left\{ x \,:\, \psi_i^n(x) < \min_{j \neq i} \psi_j^n(x) \right\}. \tag{10}$$

Benefits of Algorithm (8)-(10) include its unconditional stability (time step size δt can be chosen arbitrarily large, constrained only by accuracy considerations), seamless handling of topological changes in any dimension (the algorithm is the *very same* three simple steps shown in both two and three dimensions), and very low per time step cost ($O(N \log N)$ on a uniform grid of N points, using the FFT to compute the convolutions in step (8)). Yet, despite its extreme simplicity, it handles automatically and correctly all the essential features of the dynamics, including Herring angle conditions (5) along junctions, and countless types of topological changes that may occur during the evolution. Note that algorithm (8)-(10) can be seen as a type of level set method, where the function

$$-\psi_i^n(x) + \min_{j \neq i} \psi_j^n(x)$$

plays the role of the level set function depicting the shape of the i-th grain at the $(n+1)$-th time step.

It turns out that this simplest of algorithms from [9] results in a misorientation dependent mobility $\mu_{i,j}$ associated with the boundary $\Gamma_{i,j}$ between grains i and j that is given by

$$\mu_{i,j}(\theta_i, \theta_j) = \frac{1}{\sigma(\theta_i, \theta_j)} \tag{11}$$

leading to the normal speed

$$v_{i,j}(x) = \mu_{i,j}(\theta_i, \theta_j) \sigma(\theta_i, \theta_j) \kappa_{i,j}(x) = \kappa_{i,j}(x)$$

at any point $x \in \Gamma_{i,j}$. Although this is perhaps a rather unusual choice of misorientation dependence for the mobility of a grain boundary (experimental measurements as well as molecular dynamics simulations reported in [24] imply that grain boundary mobility in fact diminishes as surface tension does), numerical investigations in [25] indicate that many important grain statistics do not seem to depend strongly on the choice of mobilities. There is in fact a more general algorithm given in [9] that allows arbitrary choice of mobilities, but that version requires an additional step (referred to as "retardation" in [9]) that adds to the computational cost of the algorithm (although the $N \log N$ complexity remains). Here, in the interest of keeping the algorithm as simple as possible, we stick with (11).

To explore possible effects of grain rotation on size distribution, we supplement Mullins' evolution equations (4) & (5) – which are obtained by carrying out gradient descent on energy (1) with respect to the grain boundaries $\Gamma_{i,j}$ – by carrying out gradient descent on (1) also with respect to the grain orientations θ_i, which now become time dependent. Variation of (1) with respect to θ_i leads to

$$\theta_i'(t) = -\tilde{\mu}_i \sum_{j \neq i} \frac{\partial \sigma}{\partial \xi} \left(\theta_i(t), \theta_j(t)\right) \text{Length}(\Gamma_{i,j}) \tag{12}$$

where $\tilde{\mu}_i$ denotes a mobility factor associated with the rotation of the i-th grain in the network. The summands in (12) can be interpreted as torques on the i-th grain applied by its neighbors. The overall neighborhood configuration of a grain thus can have a dramatic impact on whether the grain can rotate towards one of its neighbors. The rotational mobility of a grain may have a complicated dependence on its size and its neighborhood configuration. For simplicity, here we will prescribe it to depend only on the size of the grain:

$$\tilde{\mu}_i = \frac{1}{A_i^p(t)} \tag{13}$$

where $A_i(t)$ denotes the area of the i-th grain at time t, and $p \geq 0$ is a constant. Molecular dynamics simulations of grain rotation for an embedded circular grain in [26] imply the exponent $p = 2.1 \pm 0.6$, and PFC simulations of the same setup in [27] are consistent with $p = 2$. As indicated in [26], other values for p have also been reported in earlier studies, e.g. $p = 0, 2, 3, \ldots$;see the references therein. In this paper, we will report simulations with $p = 1$, and $p = 2$ using the model described above. With our choice of rotational mobility, the rate of grain boundary migration and grain rotation for a circular embedded grain scale with respect to its radius r as

$$v \sim \frac{1}{r} \text{ and } \theta' \sim \frac{1}{r^{2p-1}}, \tag{14}$$

respectively. The exponent $p = 1$ is especially interesting: With this choice, the rate of grain rotation and grain boundary migration scale the same (i.e. as $\frac{1}{r}$) with respect to grain size, and allow us to explore

the influence of grain rotation on size statistics in a regime during which grain rotation has a sustained significance. On the other hand, the exponent $p = 2$, which is consistent with the dependence of rotation rate on grain size reported in [26, 27], implies that grain rotation becomes significant at very small scales, and is negligible compared to curvature motion (migration) of grain boundaries at large scales. With this exponent, we would expect the size distribution to eventually revert back to the usual one observed in two dimensional simulations with curvature driven grain boundary migration alone. The question then is whether the size distribution resembles that from PFC simulations at early times. With either choice of the exponent p, the rotational mobility (13) is becomes singular as a grain shrinks to a point, and therefore in practice needs to be regularized at $A = 0$.

Our algorithm for simulating the proposed model of simultaneous grain rotation and grain boundary migration is as follows:

Given the initial grain shapes Σ_i^0 and orientations θ_i^0 and a time step size δt, obtain the grain shapes Σ_i^{n+1} and orientations θ_i^{n+1} at the $(n+1)$-th time step from the grain shapes Σ_i^n and orientations θ_i^n at the end of the n-th time step as follows:

1. Compute the convolutions:

$$\phi_i^n = G_{\delta t} * \mathbf{1}_{\Sigma_i^n}. \tag{15}$$

2. Compute the lengths and the areas:

$$A_i^n = \int \mathbf{1}_{\Sigma_i^n}\, dx \text{ and } L_{i,j}^n = \frac{1}{\sqrt{\delta t}} \int_{\Sigma_j^n} \phi_i^n\, dx. \tag{16}$$

3. Form the comparison functions:

$$\psi_i^n = \sum_{j \neq i} \sigma(\theta_i^n, \theta_j^n)\phi_j^n. \tag{17}$$

4. Update the grain shapes:

$$\Sigma_i^{n+1} = \left\{ x \,:\, \psi_i^n(x) < \min_{j \neq i} \psi_j^n(x) \right\}. \tag{18}$$

5. Update grain orientations:

$$\theta_i^{n+1} = \theta_i^n - \frac{\tilde{\delta t}}{(A_i^n)^p} \sum_{j \neq i} \frac{\partial \sigma}{\partial \xi}(\theta_i^n, \theta_j^n) L_{i,j}^n. \tag{19}$$

Due to the singular dependence of the Read-Shockley surface tension model (2) & (3) on the misorientation angle at 0 , the ODE system (12) and consequently step (19) of Algorithm (15)-(19) has to be supplemented by a description of what happens when $\theta_i \approx \theta_j \mod \frac{\pi}{4}$ for some $i \neq j$ with $\text{Length}(\Gamma_{i,j}) \neq 0$ in the right hand side of (12) and (19). Indeed, it may happen that $|(\theta_i(t) - \theta_j(t)) \mod \frac{\pi}{4}|$ vanishes in finite time, leading to a blow up in $\frac{\partial \sigma}{\partial \xi}$. There is a natural way to continue the evolution beyond such a singularity: Assuming that misorientation across the boundary between grain i and one of its neighbors, say grain j , converges to 0 at any given time, we merge the two grains, removing the boundary between them that by then has vanishing surface tension $\sigma(\theta_i(t), \theta_j(t))$. This seems reasonable since it would require infinite torque to increase $|(\theta_i(t) - \theta_j(t)) \mod \frac{\pi}{4}|$ once it hits zero: Once two grains coalesce, they must remain one grain for the remainder of the evolution. This appears to be the only continuation beyond the singularity that maintains energy dissipation. In simulations, we approximate this notion of solution by introducing a minimum threshold for the misorientation angle between any two neighboring grains, and merge the two grains if their misorientation gets below the threshold value. Coalescence between two grains Σ_i and Σ_j and removal of the boundary $\Gamma_{i,j}$ between them is trivial to implement in Algorithm (15)-(19) in terms of the sets Σ_i and Σ_j as follows:

$$\Sigma_i \longrightarrow \Sigma_i \cup \Sigma_j \text{ and } \Sigma_j \longrightarrow \emptyset.$$

As a side note, observe that Algorithm (8)-(10) and the first four steps (15-18) of Algorithm (15)-(19) are invariant under introduction of zero energy interfaces: Any grain can be subdivided into smaller grains; as long as their orientations are the same as their parent, the evolution of the parent network remains unaltered. This is because interfaces with vanishing surface tension do not contribute to the comparison functions formed in steps (9) and (17) of the two algorithms (those terms drop out of the sum).

3 Simulation Results

We carried out large scale simulations using Algorithm (15)-(19) in two dimensions. The initial condition, containing well over 100,000 grains for each one of the runs, was obtained from the Voronoi cells associated with uniformly distributed random points in a periodic box, at a resolution of 4096×4096 grid points. The initial orientations of the grains were also assigned at random, from a uniform distribution on $[0, 2\pi)$. Thus, in our simulations, initially there are approximately 10^5 choose $2 \approx 10^{10}$ distinct surface tensions possible in principle. During simulations with Algorithm (8)-(10), which does not incorporate grain rotation, no pair of (neighboring or otherwise) grains coalesce during the dynamics: all grains have distinct identities (differing orientations) initially and remain so until they possibly shrink and disappear. During simulations

with Algorithm (15)-(19), two neighboring grains may merge if explicitly required to do so by the coalescence criterion of our grain rotation model in Algorithm (15)-(19). The threshold misorientation value for grain coalescence used in all simulations with this model was $\approx 1.5^\circ$. It was verified that the precise value of this threshold did not make an appreciable difference (as long as it's small) in the grain statistics, since once the misorientation between two neighboring grains is small enough, it is driven down to zero very rapidly by (12) due to the singularity in (3) at $\theta = 0$. In all simulations that use Read-Shockley surface tensions (2) & (3), the Brandon angle θ_* was chosen to be $\approx 21.5^\circ$. The initial GSD for each one of our simulations is shown in the left panel of Figure 2.

In investigating the possible effects of grain rotation on GSD, a natural preliminary question is whether Read-Shockley (i.e. unequal) surface tensions in the absence of any additional effect such as grain rotation and resulting coalescences may already explain the GSD seen in [2, 3]. Our simulations of the basic grain boundary motion model (4) & (5) of Mullins using Algorithm (8)-(10) with Read-Shockley surface tensions (2) & (3) yield a GSD that is very close to the one seen in the equal surface tension case (i.e. $\sigma(\theta_i, \theta_j) = 1$ for all i, j). Despite the unusual mobilities (11) induced by our algorithms, this is in agreement with the phase field and Monte Carlo simulations of [25] where Mullins' model is simulated in two dimensions using Read-Shockley surface tensions and mobilities given by $\mu_{i,j} = 1$ as well as with mobilities given by experimentally obtained values according to which $\mu_{i,j} \to 0$ as $\sigma_{i,j} \to 0$. In other words, unequal surface tension version of Mullins' purely geometric flow model does not appear to explain the different GSD seen in [2, 3], at least over a very wide spectrum of mobilities. This is shown in the second and third (center and right) panels of Figure 2: Although there is a very slight deformation in the GSD compared to equal surface tensions, it is still very far from the experimental distribution of [2, 3].

Figure 3 shows the time evolution of the GSD resulting from our model that incorporates grain rotation and coalescence together with grain boundary migration, computed using Algorithm (15)-(19), with the choice $p = 1$ in the dependence of rotational mobility (13) on grain size. The GSD appears for the most part to be stationary in time, and closely resembles the experimental measurements reported in [2, 3]. Figure 4 shows the corresponding distributions of effective radii, again in comparison with the measurements of [2, 3], and further corroborates the close agreement. Figures 5 and 6 explore the dependence of the aforementioned results on the choice of the exponent p in (13): Figure 5 shows the evolution of the GSD with $p = 2$, and Figure 6 shows the corresponding distributions of effective radii. These distributions behave similar to the $p = 1$ case at intermediate times, but appear to drift back towards the standard distributions seen in Mullins' model at later times as the average grain size increases and consequently grain rotation becomes progressively negligible compared to boundary migration. See Figure 1 for a plot of the two mobilities used as a function of grain area.

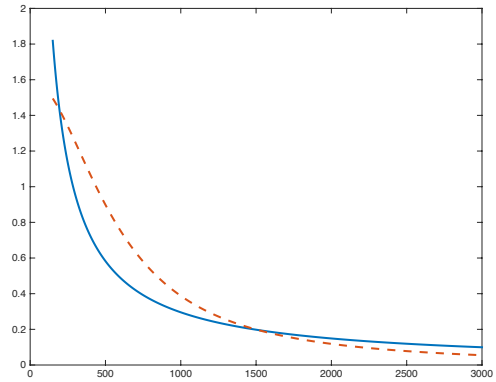

Figure 1: Plot of the two rotational mobilities used (blue & solid: $p = 1$; red & dashed: $p = 2$, with regularization) in the numerical simulations, as a function of grain area (measured in grid points).

Figure 7 shows details from the microstructures obtained from simulations with the different models considered in this paper. The first (left) panel shows zoomed view of the microstructure from Mullins' model with equal surface tensions, computed using Algorithm (8)-(10) with $\sigma(\theta_i, \theta_j) = 1$ for all i and j. As in most simulations of this familiar model, the grains are mostly convex and almost polygonal. The second (center) panel shows part of the microstructure from Mullins' model with Read-Shockley surface tensions, computed once again using Algorithm (8)-(10), but with surface tensions $\sigma(\theta_i, \theta_j)$ given by (2)-(3). Here, some differences are apparent: Read-Shockley surface tensions generate somewhat less regular (more eccentric) grains (most of which are nevertheless quite polygonal and close to being convex), and there are meandering, snake-like patterns of neighboring grains with low angle grain boundaries between them. These are in agreement with observations from previous simulations, e.g. [8], that use more natural mobilities. The considerable differences in shapes of grains apparently do not, however, translate into a difference in the size distribution. The third (right) panel shows part of the microstructure obtained from the new model presented in this paper that incorporates grain rotation and coalescence together with grain boundary migration, with $p = 1$ in (13). Now the grains are very eccentric, many of them with meandering and highly non-convex shapes. They resemble the shapes of grains seen in the PFC simulations of [1], suggesting that grain rotation and coalescences may be playing a significant role at the scales captured by that PFC simulation, and may be at least partially responsible for the observed GSD.

Finally, Figure 8 shows the effect of pure grain rotation and coalescence dynamics, in the absence of any grain boundary migration, on the GSD. The initial condition is microstructure obtained from standard Mullins' model starting with Voronoi data, which has the same GSD as shown in the rightmost plot of 2. We see that grain coalescence itself, caused by grain rotation, and not some complicated interaction between rotation and boundary migration, tends to deform the GSD towards closer agreement with the experimental distribution. In light of this and previous figures, we may conclude that grain rotation component of si-

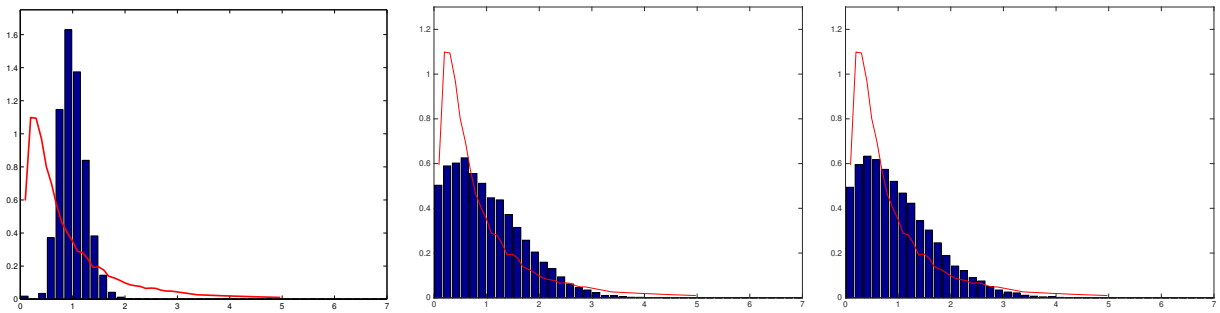

Figure 2: GSD in the initial Voronoi data, with equal surface tension Mullins' model (4) & (5), and with unequal surface tension Mullins' model and mobilities given by (11), in that order from left to right. There is very little difference between the distributions from equal and unequal surface tension versions of (4) & (5). The red curve is experimental data from [2, 3], and the bar graphs are from numerical simulations.

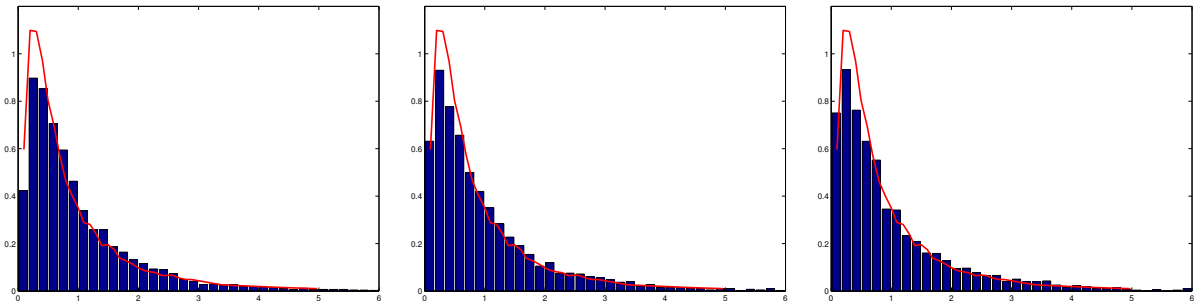

Figure 3: GSD with $p = 1$ in the expression (13) for rotational mobility. From left to right: After 25 , 50, and 75 time steps. The red curve is experimental data from [2, 3], and the bar graphs are from numerical simulations.

multaneous dynamics favors a GSD much closer to the experimental distribution, while the grain migration component favors the standard GSD seen in Mullins' model and is eventually strong enough to win over grain rotation to revert to that GSD with $p = 2$ but not with $p = 1$ in (13).

4 Conclusions

We have presented a model for simultaneous grain boundary migration and grain rotation that is obtained in a natural manner from Mullins' well known model for grain boundary motion. We also presented a novel, very efficient and extremely streamlined algorithm for its numerical simulation. We used the algorithm to carry out large scale simulations of the evolution of GSD in fiber textured thin films, both in the presence and absence of grain rotation.

The GSD in simulations with Mullins' model (no rotation) with Read-Shockley surface tensions (with two dimensional crystallography) closely resembles the one with equal surface tensions. This is in agreement

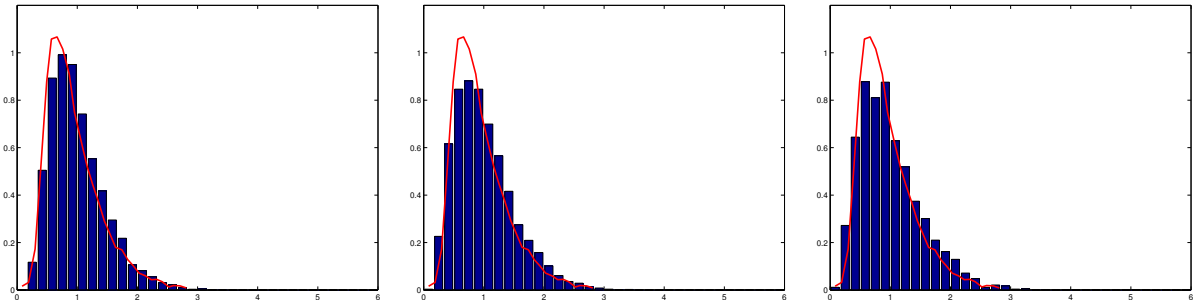

Figure 4: Normalized radii corresponding to the plots in Figure 3. The red curve is experimental data from [2, 3], and the bar graphs are from numerical simulations.

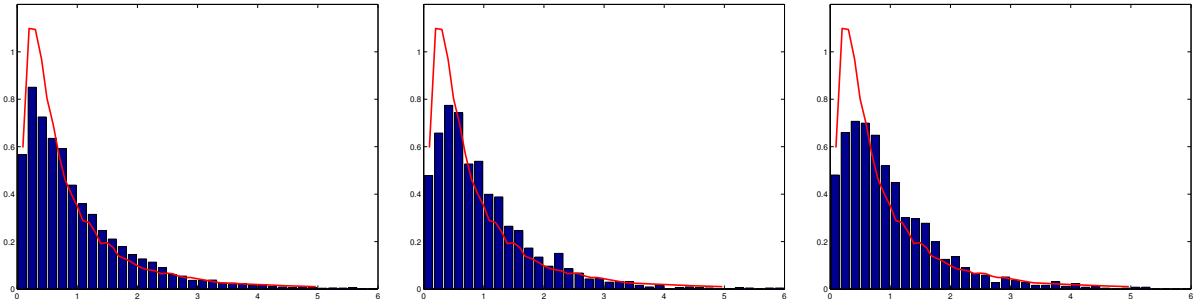

Figure 5: GSD with $p = 2$ in the expression (13) for rotational mobility. From left to right: After 25, 100, and 200 time steps. It appears that as the average grain size increases, the GSD moves back towards that of standard Mullins' model. The red curve is experimental data from [2, 3], and the bar graphs are from numerical simulations.

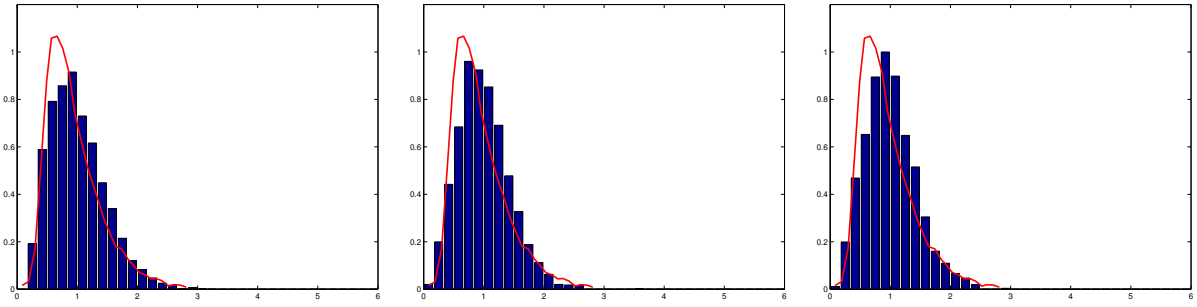

Figure 6: Normalized radii corresponding to the plots in Figure 5. The red curve is experimental data from [2, 3], and the bar graphs are from numerical simulations.

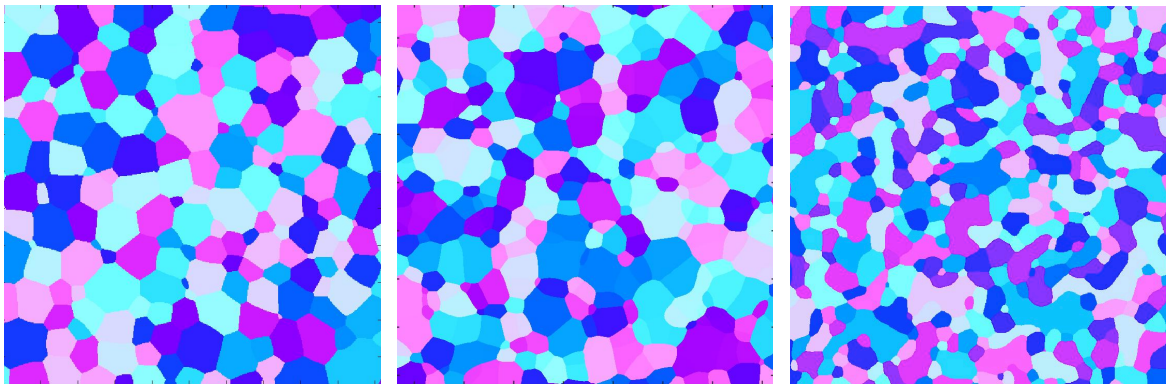

Figure 7: Details (zoomed view) of microstructure from simulations with: the equal surface tension grain boundary motion model, the unequal (Read-Shockley) surface tension grain boundary motion model, and simultaneous unequal surface tension grain boundary motion and grain rotation model, in that order. The grains shapes are very regular and almost polygonal in the equal surface tension case. With Read-Shockley surface tensions, but in the absence of grain rotation, the grains are somewhat less regular, with several in view that are fairly eccentric. Additionally, the meandering, snake-like patterns formed by neighboring grains with low angle grain boundaries between them are apparent, as was noted in previous simulations of fiber textured thin films using Mullins' model with Read-Shockley surface tensions e.g. [8]. The microstructure from the simultaneous Mullins' model with Read-Shockley surface tensions and grain rotation (with $p = 1$ in mobility 13) and resulting coalescences, on the other hand, is dramatically less regular: There are many meandering grains with high eccentricity, some with significantly larger areas. These resemble some of the unusual grain shapes seen in the PFC simulations reported in [1].

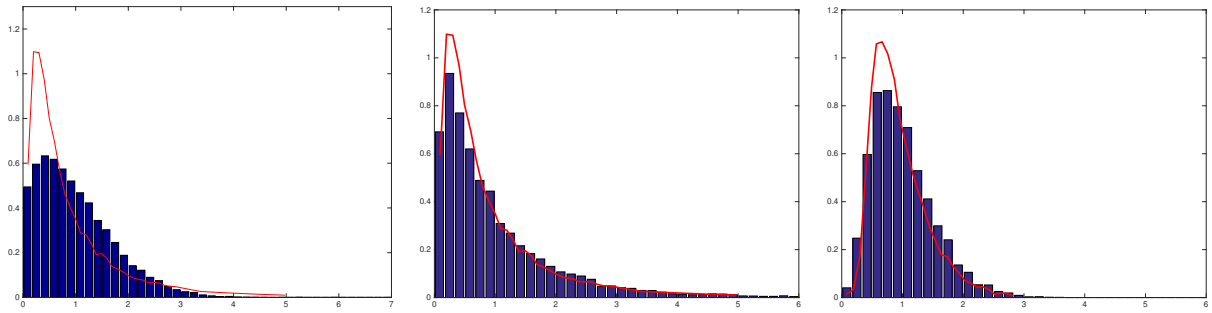

Figure 8: Effect on GSD of pure grain rotation and coalescence, in the absence of grain boundary migration. Left: Initial GSD, obtained from the pure grain boundary migration model of Mullins, as in Figure 2, starting from Voronoi data. Middle: Resulting GSD after only grain rotation dynamics and coalescences it leads to, in the absence of any grain boundary migration. Right: The distribution of normalized radii corresponding to the GSD in the middle plot.

with previous simulations despite our choice of very different mobilities. Thus, it appears that across a very wide spectrum of mobilities, GSD in Mullins' model is independent of the choice of mobility, and behaves very similarly whether using equal or Read-Shockley surface tensions.

On the other hand: The GSD in some of our simulations of simultaneous grain boundary migration and grain rotation closely matches the one observed in PFC simulations of [1], which in turn is close to the experimental GSD reported in [2, 3]. In the new model presented, grain rotation naturally leads to occasional coalescences between neighboring grains with low angle grain boundaries between them, whenever the misorientation across the boundary vanishes due to rotation and alignment. This leads to the formation of grains with eccentric shapes as seen in the PFC simulations, and appears to be responsible for the differing GSD. The resulting microstructure resembles the one that arises in PFC simulations presented in [1] in which grain rotation and coalescences are also quite apparent and frequent. Neither microstructures, however, resemble the experimental microstructure shown in [3].

This similarity of microstructures and GSD between our simulations and PFC simulations of [1] suggests that grain rotation and coalescences may be at least partially responsible for the success PFC has had in reproducing the experimental GSD of [2, 3]. On the other hand, the unusual microstructure seen in these simulations suggests that the parameter regime used in the simulations (e.g. the size of the grains in the PFC simulation, or the rotational mobilities used in our continuum model) may allow or encourage grain rotation and coalescence more readily and frequently than what is relevant for the experimental set up of [2, 3]. If so, it may be interesting to carry out atomistic simulations in a regime (e.g. with larger grains) that limits coalescences in order to assess whether other effects it might be capturing, such as triple junction drag as was recently considered in [23] in the context of a continuum model, would also allow it to reproduce a similar GSD.

The model of grain rotation and coalescence presented here incorporates these effects into Mullins' continuum model of grain boundary migration in a very simple, phenomenological manner, by liberating additional pathways in the energy landscape for the dissipation of Mullins' energy via perturbations to the grain orientations. It therefore cannot be expected to faithfully reproduce detailed atomistic underpinnings of these processes. Indeed, in the model presented, an embedded circular grain with small misorientation would always rotate to monotonically decrease its misorientation as it shrinks, whereas the analysis in [5] indicates that grain rotation with embedded grains can take place in a direction that increases the misorientation angle as well as the energy density (energy per unit length), while maintaining total energy dissipation (due to shortening of the grain boundary). PFC simulations in [27] corroborate this analysis. In addition, unlike in the experiments of [2, 3], grain growth will never stagnate in the model presented here. Finally, it is worth repeating that the mobilities associated with grain boundary migration that result from the simple

algorithms used in this paper are quite unusual. Indeed, molecular dynamics simulations using Monte Carlo and phase field methods reported in [24] indicate that mobility of grain boundaries diminish with misorientation. In our defense on this point, numerical experiments using both Monte Carlo and phase field methods reported in [25] suggest that certain statistics of the microstructure, such as the GSD, appear for the most part to be independent of the choice of mobilities.

In summary, despite their limitations, our simple model and simulations suggest at the very least that grain rotation induced coalescence and the resulting elimination of very low angle grain boundaries seen in PFC simulations appear to be relevant for the different GSD obtained in those simulations from the usual one seen in the standard version of Mullins' continuum model.

Acknowledgment: This work was supported by NSF DMS-1317730.

References

[1] Backofen, R. Barmak, K.; Elder, K. E.; Voigt, A. *Capturing the complex physics behind universal grain size distributions in thin metallic films.* Acta Materialia. **64** (2014), pp. 72-77.

[2] Barmak, K.; Kim, J.; Kim, C.-S.; Archibald, W. E.; Rohrer, G. S.; Rollett, A. D.; Kinderlehrer, D.; Ta'asan, S.; Zhang, H.; Srolovitz, D. J. *Grain boundary energy and grain growth in Al films: Comparison of experiments and simulations.* Scripta Materialia. **54** (2006), pp. 1059-1063.

[3] Barmak, K.; Eggeling, E.; Kinderlehrer, D.; Sharp, R.; Ta'asan, S.; Rollett, A. *Grain growth and the puzzle of its stagnation in thin films: the curious tale of a tail and an ear.* Prog. Mater. Sci. **58** (2013), pp. 987.

[4] Brandon, D. G. *The structure of high-angle grain boundaries.* Acta Metallurgica. **14** (1966), pp. 1479-1484.

[5] Cahn, J. W.; Taylor, J. E. *A unified approach to motion of grain boundaries, relative tangential translation along grain boundaries, and grain rotation.* Acta Materialia. **52** (2004), pp. 4887-4898.

[6] Elder, K.; Katakowski, M.; Haataja, M.; Grant, M. *Modeling elasticity in crystal growth.* Phys. Rev. Lett. **88**:24 (2002).

[7] Elsey, M.; Esedoglu, S.; Smereka, P. *Diffusion generated motion for grain growth in two and three dimensions.* Journal of Computational Physics. **228**:21 (2009), pp. 8015-8033.

[8] Elsey, M.; Esedoglu, S.; Smereka, P. *Simulations of anisotropic grain growth: Efficient algorithms and misorientation distributions.* Acta Materialia. **61**:6 (2013), pp. 2033-2043.

[9] Esedoglu, S.; Otto, F. *Threshold dynamics for networks with arbitrary surface tensions.* Communications on Pure and Applied Mathematics. **68**:5 (2015), pp. 808-864.

[10] Harris, K. E.; Singh, V. V.; King, A. H. *Grain rotation in thin films of gold.* Acta Materialia. **46**:8 (1998), pp. 2623-2633.

[11] Haslam, A. J.; Phillpot, S. R.; Wolf, D.; Moldovan, D.; Gleiter, H. *Mechanisms of grain growth in nanocrystalline fcc metals by molecular-dynamics simulation.* Materials Science and Engineering A. **318** (2001), pp. 293-312.

[12] Haslam, A. J.; Moldovan , D.; Phillpot, S. R.; Wolf, D.; Gleiter, H. *Combined atomistic and mesoscale simulation of grain growth in nanocrystalline thin films.* Computational Materials Science. **23** (2002), pp. 15-32.

[13] Herring, C. *Surface tension as a motivation for sintering.* In The Physics of Powder Metallurgy. W. Kingston, Ed. McGraw-Hill, New York, 1951, pp. 143-179.

[14] Holm, E. A.; Hassold, G. N.; Miodownik, M. A. *On misorientation distribution evolution during anisotropic grain growth.* Acta Materialia. **49** (2001), pp. 2981-2991.

[15] Kinderlehrer, D.; Livshits, I.; Ta'asan, S. *A variational approach to modeling and simulation of grain growth.* SIAM J. Sci. Comput. **28**:5 (2006), pp. 1694-1715.

[16] Merriman, B.; Bence, J. K.; Osher, S. J. *Diffusion generated motion by mean curvature.* Proceedings of the Computational Crystal Growers Workshop. (1992).

[17] Merriman, B.; Bence, J. K.; Osher, S. *Motion of multiple junctions: a level set approach.* Journal of Computational Physics. **112** (1994), pp. 334-363.

[18] Moelans, N.; Spaepen, F.; Wollants, P. *Grain growth in thin films with a fiber texture studied by phase-field simulations and mean field modelling.* Philosophical Magazine. **90**:1 (2009), pp. 501-523.

[19] Moldovan, D.; Yamakov, V.; Wolf, D.; Phillpot, S. R. *Scaling behavior of grain-rotation-induced grain growth.* Physical Review Letters. **89**:20 (2002), pp.

[20] Lobkovsky, A.; Warren, J. A. *Sharp interface limit of a phase-field model of crystal grains.* Physical Review E. **63** (2001).

[21] Mullins, W. W. *Two dimensional motion of idealized grain boundaries.* J. Appl. Phys. **27** (1956), pp. 900-904.

[22] Read, W. T.; Shockley, W. *Dislocation models of crystal grain boundaries.* Physical Review. **78**:3 (1950), pp. 275-289.

[23] Streitenberger, P.; Zollner, D. *Triple junction controlled grain growth in two-dimensional polycrystals and thin films: Self-similar growth laws and grain size distributions.* Acta Materialia. **78** (2014), pp. 114-124.

[24] Upmanyu, M.; Srolovitz, D. J.; Shvindlerman, L. S.; Gottstein, G. *Misorientation dependence of intrinsic grain boundary mobility: simulation and experiment.* Acta Materialia. **47**:14 (1999), pp. 3901-3914.

[25] Upmanyu, M.; Hassold, G. N.; Kazaryan, A.; Holm, E. A.; Wang, Y.; Patton, B.; Srolovitz, D. J. *Boundary mobility and energy anisotropy effects on microstructural evolution during grain growth.* Interface Science. **10** (2002), pp. 201-216.

[26] Upmanyu, M.; Srolovitz, D. J.; Lobkovsky, A. E.; Warren , J. A.; Carter, W. C. *Simultaneous grain boundary migration and grain rotation.* Acta Materialia. **54** (2006), pp. 1707-1719.

[27] Wu, K.-A.; Voorhees, P. W. *Phase field crystal simulations of nanocrystalline grain growth in two dimensions.* Acta Materialia. **60** (2012), pp. 407-419.